International Journal of Scientific Engineering and Applied Science (IJSEAS) – Volume-4, Issue-03, March 2018
ISSN: 2395-3470
www.ijseas.com

Application of X-Ray Spectroscopy to Thermal Flaws Detection in Solid Rocket Motor Combustion Chamber

Gbadebo Omoniyi Adeniyi[1], Sergey Konstantinovich Savelyev[2], Oluwole Olalekan Peters Onibon-oje[1], Emmanuel, Nnali-Uroh[1], Olufunke Ayomikun Aiyegbusi[1]

[1]*National Space Research and Development Agency (NASRDA), P.M. B 437, Abuja, Nigeria*
Center for Space Transport & Propulsion (CSTP), Epe P.M.B 1001 Lagos, Nigeria

[2]*Baltic State Technical University, Saint Petersburg, Russia*

Abstract

This paper presents the application of a software package called x-ray model. The package demonstrates the behavior of an x-ray machine in analyzing and detecting thermal flaws in rocket combustion chamber.

The model was used to analyze thermal flaws resulting from high temperature gas produced during combustion. These analyses were based on density variation as the high temperature gases interacting with the chamber insulating materials. Fiber glass, polyurethane and epoxy materials were analyzed. Visual observation of thermal flaws at different x-ray energy levels was also presented.

The x-ray model is a reliable and precise way of analyzing thermal destruction in rocket engines.

1. Introduction

Thermal defect in rocket combustion chamber is a serious problem associated with heat dissipation towards the chamber wall during propellant combustion. The presence of un-burn solid propellant particles in a high temperature gas flow generated during combustion strongly affects the gas-surface interaction [32]. In this process, the thermo-chemical and dynamic impact from the gas phase is aggravated by the erosive attachment from the dispersed phase, contained in the gas. Near the streamlined surface, gas dynamic, thermal and erosion phenomena are strongly interconnected. Even small concentrations of particles in a gas flow significantly intensify heat transfer, increase thermo-chemical destruction, and give a change in the regime of flow of the surface film of the melt. [29].

Heat destruction of chamber wall and propellant casing could result from the following internal processes during flow: loading by internal pressure, convection from moving media to destructing rough material, radiation heat flux, transfer of heat to wall by particle sedimentation, impact of particles with a wall and heat of materials and gas flow. These complex mechanisms have certain specific features that distinguish them from the limiting cases of thermal and erosive destruction taken alone. Therefore, analyzing the thermal defect of rocket chamber and propellant casing using specialized x-ray software is a promising effort towards a successful rocket design. The figure 1 illustrates the sectional and cross-sectional view of a typical solid rocket chamber showing the propellant, propellant casing and chamber wall.

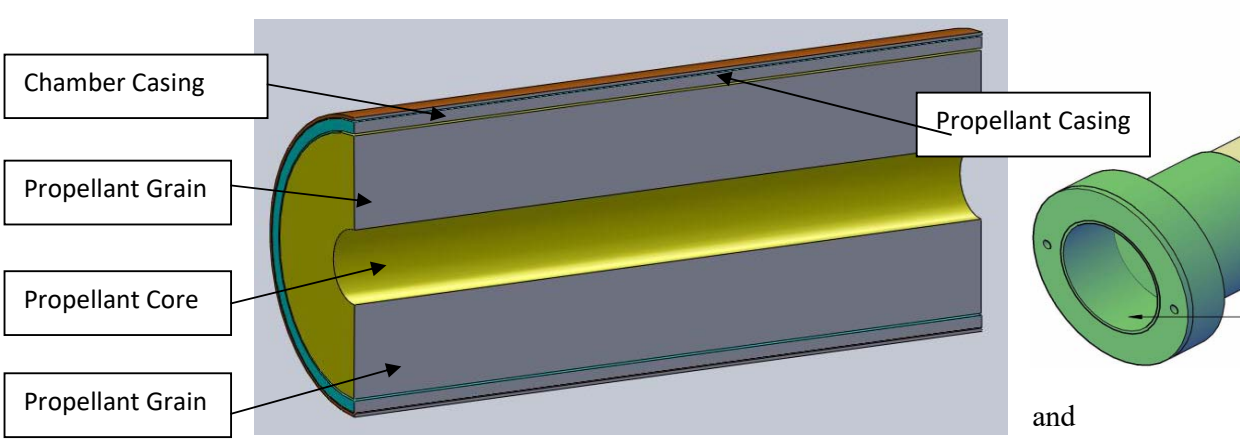

and cross-sectional view of a typical rocket chamber

1.1 Problem Definition

Thermo-chemical processes on the chamber surface, which is flowed over by a high temperature gas, have been studied since the origin of the space or airspace industry. Different well founded simulation possibilities for analyzing heat destruction of materials using conventional computational models have been carried out [17; 30; and 35]. However, analysis of heat defect in high temperature dusted gas dynamics using x-ray spectroscopy has been found to be perfect and more accurate compared to conventional simulation. This is because of the presence of uncertainties of unacceptably high order having been reported when conventional computer-aided and simulation codes, are attempted for the analysis. This is brought about as a result of extreme variations in temperature, pressure and velocity between the phases and also temporarily along the chamber. However, this facility has not been fully and successfully employed for detecting thermal flaws. This approach is non-intrusive to the acquisition of local measurements of defect, cracks or volume fractions in the chamber and propellant.

Prediction of gas-solid flow fields, in aerospace applications such as combustion and other internal flows are crucial. Therefore, one of the most important tools for improving our understanding of this analysis is by developing a high level and specialized model which describe or simulate the behavior of x-ray machine appropriate for this investigation.

2. Application of X-ray Spectroscopy

Visualization of the internal gas flow dynamics of high temperature dusted gas flow and heat destruction analysis has been one of the important goals in propulsion system. The technique can be used for examination of flow behaviors, parameters distributions, defects and cracks in the duct in their full three dimensional perspective. Based on this logic, a measurement technique called X-ray test inspection has been developed. Among several instruments for the measurement of thermal defects and associated parameters, X-ray test

inspection technique has the following advantages: it is a low cost technique; it is suitable for transient measurement; large variations of flow design accommodates making the method appropriate for different flow situations and geometry; both intrusive and non-intrusive measurements are possible; point measurement as well as global measurement can be made by suitable design of the probe; and same principle (sometimes the same probe) may be used for the measurement of associated parameters like flow regime identification; particle size and shape and phase velocity. X-rays have been used for such purpose with each having its own unique properties and area of application. Availability of instant high quality digital radiographic images helps in quick inspection, transmission over network, archiving information in minimal space and the availability of sophisticated image processing algorithms for analyzing the data.

X-ray tomography as a precision method of materials characterization and defect location to ensure high reliability of aerospace engines and conformance to design requirements. This sophisticated and proven technology is employed for non-destructive evaluation (NDE) of materials and structures [6]. X-ray tomography can be used to produce both two-dimensional and three-dimensional images of structures, materials, parts, and components [42]. These images are providing information that is useful for inspection, evaluation, and diagnostics of complex hardware. X-ray test facility has a wide application in several investigations of solid rocket motor (SRM), space shuttle main engine (SSME), and solid propulsion integrity program (SPIP), modified NASA motor program, and sub-scale solid rocket combustion simulator, and other aerospace and aerospace-related applications. X-ray tomography uses high intensity X-ray sources, sensitive electronic detectors, sophisticated computer control and analysis techniques, and automated manipulation systems capable of translating and rotating test objects, to produce cross-sectional images of precision aerospace components and processes. This test method can be used to verify tolerances, determine relative material densities, locate inclusions or defects, and measure the extent of erosion and ablation in composite materials in aerospace flying vehicle. The equipment and procedure is applicable to metals, composites, or combination metal/composite structures. Cross-sectional images, generated by rotating and translating test objects slowly in an X-ray source, produce accurate representations of thin slices of the test object. It takes 20 minutes to produce an image of a thin slice. The entire process is controlled remotely by computer. Operational personnel are located external to the test cell.

A principal use of X-ray tomography has been used in evaluation of solid propellant rocket motor nozzles. The technique has been used for verification of nozzle integrity, thermocouple location determination, and post-fire char depth evaluation. The procedure can locate high or low density inclusions, delaminations, or debonds, and profound material density variations. The images can be observed in near real time as they are generated, and are archived for future detailed analysis and evaluation. Several X-ray testing approaches have been developed and used for solving many aerospace problems. One method developed at the University of Florida is based on penetrating X-ray photons. The typical energy for X-ray photon used in this kind of experiment is between 20keV and 200keV which is larger than the visible photon energy that is around some 75keV [51].

Projection Radiography (Fig. 2) is the first method developed using penetrating photons. It is based on the interaction of photons inside the material. Photons are more or less absorbed depending on the density of electrons of the tested sample. A sensitive film is

placed behind the sample on the opposite side of the X-ray source and it shows variations in intensity due to density difference inside the material.

A different technique, called Compton Backscattering Imaging (CBI) is based on backscattered photons. The information is not given by photons which pass through the sample like in transmission radiography, but is given by photons which are reflected back on the same side of the source. A CBI system operates somewhat like an optical visual system where the reflected photons from surfaces of the objects are employed to form an image of the object. All existing CBI systems rely on penetrating photons (X-rays or gamma rays) which have had only a single scatter in the object to form an image [9]. Object surface irregularities and internal in-homogeneities obstruct and corrupt such first-scatter dependant techniques. Highly localizing collimators on X-ray generator and scatter field detectors, as well as slow-running, complex image data algorithms are required to extract useful structure information. This leads to high source strength and slow imaging system operation.

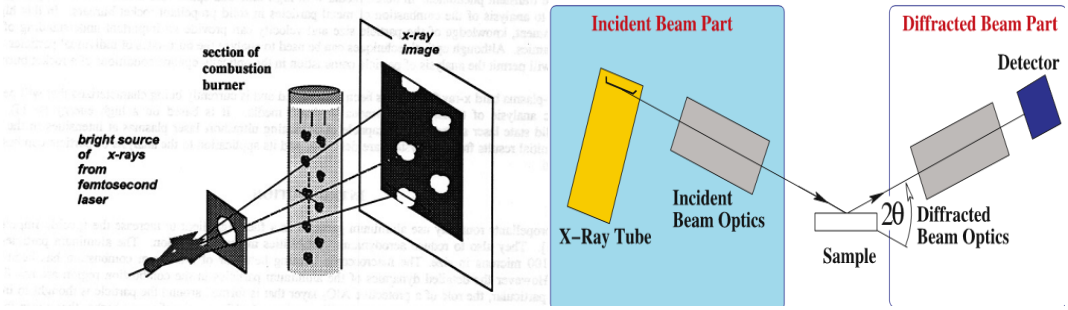

Fig. 2 X-ray projection radiography and backscattering approaches [44]

Lateral Migration Radiography (LMR) (Fig. 3) is similar to the CBI technique, but instead of counting only single backscattered photons, the LMR technique counts both single and multiple scatter photons. It selects the photons coming back. LMR is a new form of Compton backscatter imaging (CBI) that utilizes both multiple-scatter and single-scatter photons. This modality uses the lateral transport of scattered photons in materials to form images. The technique of LMR is a new imaging modality developed at UF which uses the lateral transport of both single and multiple scattered photons to form separate images.

Large area detectors operating in the current or integration mode rather than in the voltage or counting mode help to reduce the required X-ray source strength and image acquisition time. LMR systems use two types of detectors to form images. Un-collimated detectors sense predominantly first-collision photons and primarily generate images of surface or near-surface features. Properly positioned collimated detectors sense predominantly multiple-collision photons. The contrast in the collimated detector images is due to multi-scattered photon lateral transport which is sensitive to the electron density of the transport medium as well as the surface spatial details. This enables us to image, with high photon collection efficiency, objects that contain clusters of subtle

imperfections and discontinuities in electron density and identify such electron density differences.

The multiple-collision photons always carry the information of the first collision. However, with the increase in the number of collisions, multiple-collision components average out small-sized electron density variations while retaining the information from the large-size discontinuities.

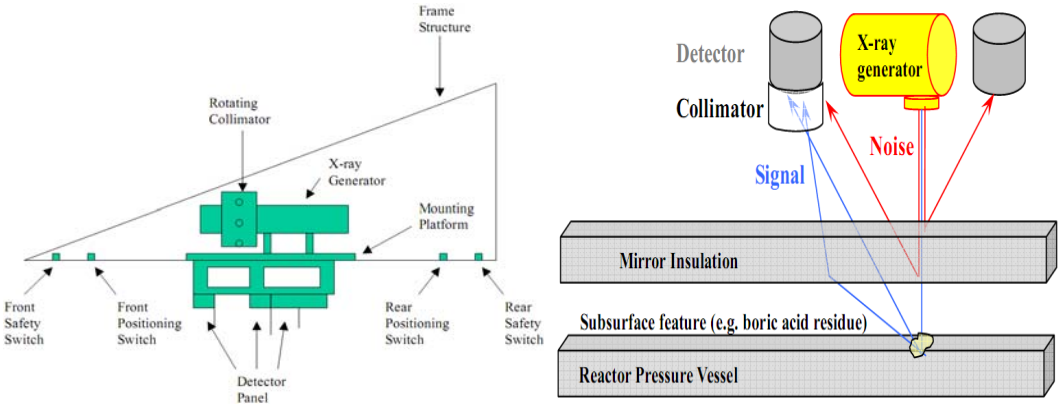

Fig. 3 Lateral migration radiography and radiography by selection detection approaches [4]

Because the LMR images are no longer restricted to first-scatter photons, this modality is useful for imaging objects even in the presence of surface clutter with high photon detection efficiency. The length of the collimator is adjusted to block first collision photons from reaching the collimated detector. The contrast in the collimated detector images is due to multiple-scattered photon lateral transport that is sensitive to the electron density of the transport medium as well as the surface spatial details. This enables us to create an image of objects that contain clusters of subtle imperfections and discontinuities in electron density and identify such electron density differences. Therefore if an air gap is present in the target, the photons are going to stream down the gap and after further collisions they will be detected with an enhanced probability by the collimated detector. The flaw detection system consists of an X-ray source and several detectors, some collimated and some un-collimated, placed around the source. The setup for the flaw detection project is simpler. The un-collimated detector is used to create an image of the surface irregularities. The X-ray collimator tube enables the user to have a narrow beam focused on the sample. The size of the incident beam can be changed and hence, scan the exposed area. This gives us the ability to modify the pixel size and to a degree, the resolution of the image.

Radiography by selective detection (RSD) is another new type of X-ray Compton backscatter imaging (CBI) where different components of the X-ray backscatter field are preferentially selected to enhance the contrast and detection of specific features. A variant of this technique, called lateral migration radiography (LMR). RSD has the ability to detect voids, and air spaces. As a result, RSD can be applied to the detection of features such as: cracks, voids, delaminations and corrosion. A wide variety of materials

have been imaged including: aluminum, plastics, honeycomb structures, steel reinforced carbon-carbon composites (RCC), concrete and titanium.

Most recently, an RSD scanning system is being used by Lockheed Martin Space Systems Co. and NASA to detect defects in the spray-on foam insulation (SOFI) used on the external fuel tank of the space [4]. The X-ray backscatter RSD approach is based on image contrast induced by varying electron densities along the photon path. Changing features cause photons to be scattered, absorbed or streamed along their path to the detector. Each of these interactions results in changes in the detector response. These changes in detector response are collectively used to generate an image, where changes in field intensity (count rate or voltage) are visually represented as changes in image contrast. Backscatter RSD selectively detects X-rays that enhance the image signal-to-background ratio allowing for the detection of features, which may otherwise go undetected using conventional CBI or transmission radiography. Noise can be subtracted from the image using other detectors, or rejected through the use of collimators. Possible features of interest can be: cracks, corrosion, voids, delaminations, hidden objects, or improvised explosive devices (IEDs). Inspection of these areas can be troublesome, especially if mirror insulation must be removed. Current RSD X-ray backscatter techniques can be used to inspect RPV penetrations without removing mirror insulation.

3. Description of the Model

The model is called X-ray simulation model. It is a model which simulates the behavior of an x-ray machine in detecting density variation caused by heat destruction in the combustion chamber. The basic principle of this code is that it does all the analysis based on density variation to detecting thermal defect of chamber material under high temperature dusted gas flow (Fig.4).

The code simulates a high temperature dusted gas flow in the duct provided by the grain with insulating material at the wall. It is based on the backscattering analysis of X-ray photons penetrating through the material. The code's interface is calibrated in millimeters (0-500mm in (x) (length) and 0-300mm (y) (thickness) while the angles are in degrees. The code also has the following X-ray properties as its input data: The X-ray beam incident angle, the backscattering angle and the number of iteration. The mass absorption coefficient of the propellant grain and that of the chamber materials (Tau) ($mm^2.g^{-1}$), the backscattering coefficient of the propellant grain and that of the chamber materials (Ba) ($mm^2.g^{-1}$), the density of the propellant grain combination and that of the chamber materials (Den) $kg.m^{-3}$ and with a graphical interface for plotting X-ray intensity(I) against distance(x). In the interface of the software, the blue section represents the chamber casing and propellant casing while the other section beneath it is the propellant grain.

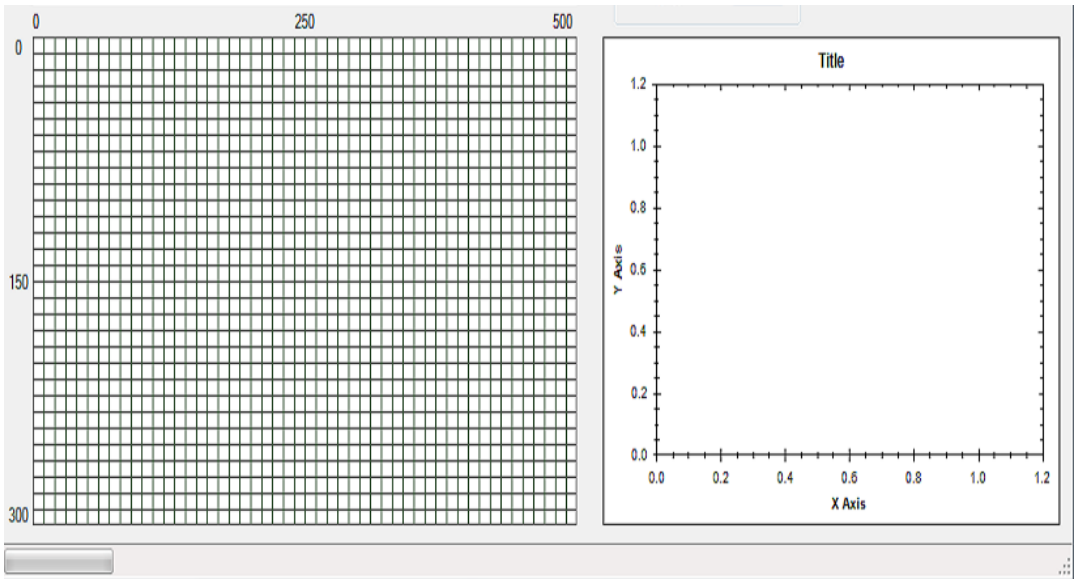

Fig. 4 X-ray simulation model

4. Simulation

This software demonstrates the backscattering behavior of x-ray machine in investigating interaction of the combustion gas, produced from propellant burning with the chamber wall and propellant casing.

Thermal defects were created at different depths, while high temperature dusted flow were simulated around the defects. The X-ray incident angle was taken to be 0 degree, backscattering angle also 0 degree, and the number of iteration was taken as 500. The grain combination used for this simulation was made of: Potassium nitrate (KNO_3) = 72 %, Aluminum (Al) = 4 %, Iron (II) Oxide (Fe_2O_3) = 1 % and Epoxy (Binder) = 23 %. The Grain X-ray properties at two different energy levels adopted in this investigation were shown in table 1. Meanwhile, the types of casing investigated were: Fiber glass (S_iO_2), Epoxy ($C_9H_{10}O_3$) and Foam Polyurethane ($CH_3NHCO_2CH_2CH_3$) with X-ray properties and densities given in table 2.

The casing dimensions investigated were: 497mm by 58mm and 497mm by 98mm (length by thickness) (fig. 5 and 6; and 7 respectively). The thermal defects resulting from high temperature gas flow within the wall were positioned at the following depths for the simulations : 79mm by 18mm, 179mm by 30mm, 289mm by 39mm, 419mm by 56mm and 496mm by 18mm (thickness by depth) (Fig. 5). Then, the x-ray model executed to determine the possibility of detecting density variations in the wall. The sensitivity of x-ray beams to casing material density and thermal defects at different depths were also determined.

Table 1: The Grain X-ray Properties at Two Different Energy Levels and Density

Energy Level(MeV)	Scattering Coefficient $\left(mm^2/g\right)$			Mass Absorption Coefficient (Tau) $\left(mm^2/g\right)$	Density (ρ_p) $\left(kg/m^3\right)$
	Coherent Scattering	Incoherent Scattering	Backscattering Coefficient(Ba)		
3.00E+00	1.35E-03	3.49	3.49135	5.88E-04	1780
3.00E+03	1.35E-09	1.33E-02	1.33E-02	3.84E-07	

[34]

Table 2: The Insulating Materials X-ray Properties and Densities

Insulating Material Type	Energy Level (MeV)	Scattering Coefficient $\left(mm^2/g\right)$			,Mass Absorption Coefficient (Tau) $\left(mm^2/g\right)$	Densities (Den) $\left(kg/m^3\right)$
		Coherent Scattering	Incoherent Scattering	Backscattering Coefficient (Ba)		
S_iO_2	3.00E+00	1.25E-02	3.47	3.47125	3.07E-04	5670
	3.00E+03	1.25E-09	1.32E-02	1.33E-02	2.06E-07	
$C_9H_{10}O_3$ (Epoxy)	3.00E+00	4.83E-04	3.68	3.690483	3.33E-05	1250
	3.00E+03	4.83E-10	1.40E-02	1.40E-02	2.33E-08	
$CH_3NHCO_2CH_2CH$ Polyurethane Foam	3.00E+00	4.95E-04	3.77	3.770495	3.61E-05	640
	3.00E+03	4.95E-10	1.44E-02	1.44E-02	2.52E-08	
Vacuum	Any energy level	0.00	0.00	0.00	0.00	0.00

[34]

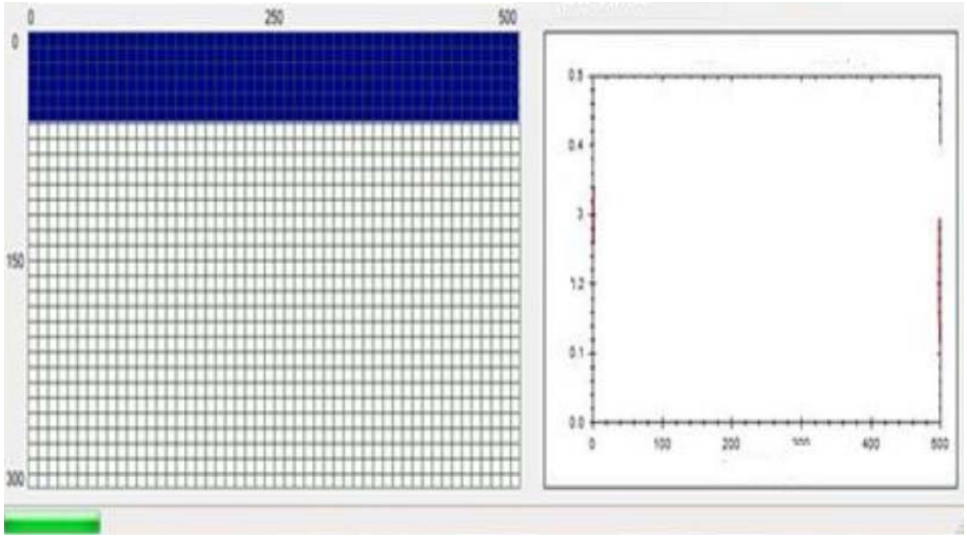

Fig. 5 Chamber wall (497 mm by 18 mm) without thermal defect

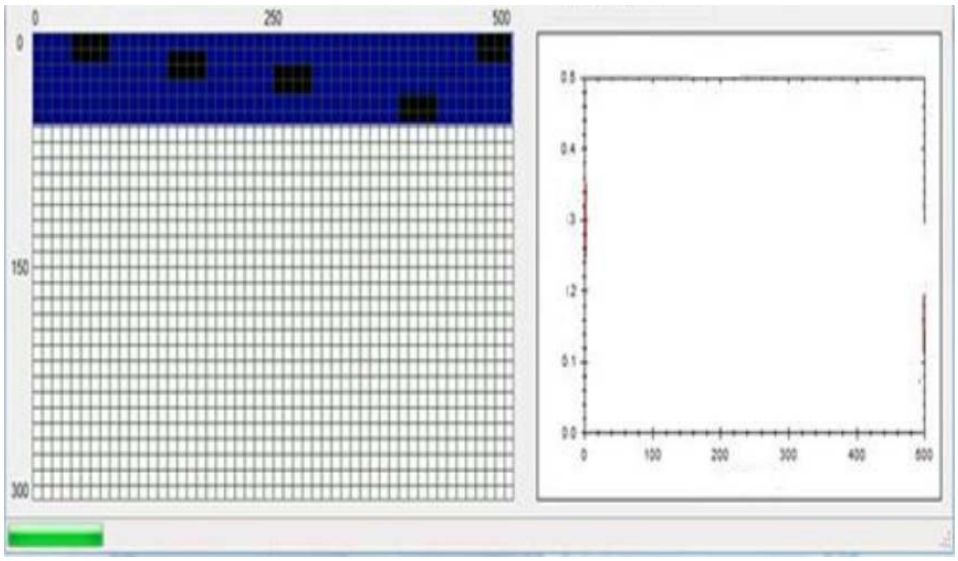

Fig. 6 Thermal defects (79mm by 18mm, 179mm by 30mm, 289mm by 39mm, 419mm by 56mm and 496mm by 18mm) at different depths within the chamber wall (497mm by 18mm)

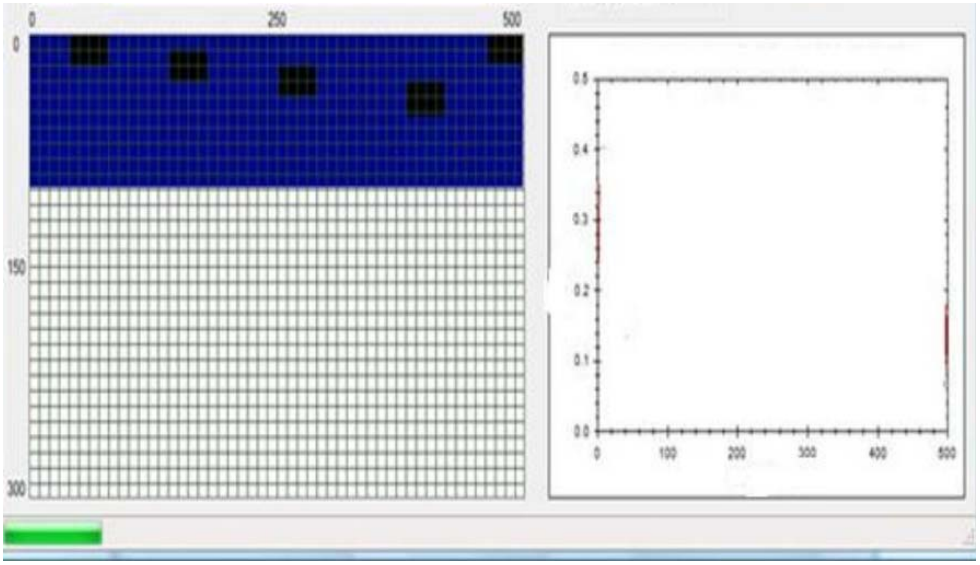

Fig. 7 Thermal defects (79mm by 18mm, 179mm by 30mm, 289mm by 39mm, 419mm by 56mm and 496mm by 18mm) at different depth within the chamber wall (497mm by 98mm)

7. Result and Analysis

X-ray backscattering technique is used to investigate the sensitivity of X-ray beam to detecting discontinuity in density of chamber materials used in rocket engines. Variation in density of material according to this technique signifies the presence of thermal defect in such material. At this region, the energy of the X-ray photons is absorbed (lower intensity or intensity drop) leaving the backscattering photons with less energy. Figure 8a (I) shows the probability of backscattering photons in fiber glass (density $5670\,kg/m^3$). The X-ray energy intensity is about 0.41 eV and uniform density is observed in the material. This indicates that material has no defect at the beginning of the investigation (no X-ray energy is absorbed and there is high level of backscattering). Figure 8a (II) shows drops in X-ray beam intensity at different locations within the wall (meaning x-ray photon energy is absorbed). This is an evidence of discontinuity in density at these locations and which signify the presence of thermal defects (less backscattering energy) caused by heat transfer from high temperature gas flow. Also, the X-ray beam intensity is observed to increase with the increase in depth of the thermal defects. Indicating that backscattering tendency is function of how deep the defects are within wall.

Figure 8b shows the implication of casing thickness on the sensitivity of the X-ray beam to density variations. Figure 8b(I) shows that X-ray backscatterring energy intensity($0.61\,eV$) increases with increasing fiber glass thickness. It is also observed that due to increase in material thickness, lesser X-ray photons energy is absorbed at the defects locations (Fig.8b(II)) compared to the earlier results. Meaning that backscatterring increases with increase in casing thickness and also seen to increase with increase in depth of the defects as ealier explained.

Figure 8c reveals the effect of higher X-ray energy level (3.00E+03) on density variation detection technique. The earlier investigation was based on X-ray energy of 3.00E+00.

Probabilty of energy absorption decreases with higher X-ray energy level. The tendency of coherent scatterring reduces too. Meanwhile, in–coherent scatterring is more pronouced.

Similar investigations were carried out using epoxy material instead of fiber glass. This is to have the understanding of the behavoiur of the material density variation using the same technique. Epoxy is a material of lower density (1250kg/m^3), thus the intensity of the backscatterring energy is lower compared to fiber glass ($0.20\,eV$)(Fig.9a (I)). Meaning that scatterring increases with decreasing density of the material. Also, similar explanations given earlier in (Fig.8b) apply here too. Backscatterring is also noticed to increase with material thickness and increase in depth of defects (Fig.9 (I-II)). The effect of X-ray photons backscatterring (in-coherent) is also pronounced with higher X-ray energy level using epoxy material (Fig.9.c).

Polyurethane foam is a special material with density, 640kg/m^3. The backscattering photons within the material and with increasing defect depths are also shown in figure 10. The detailed explanations are as stated earlier.

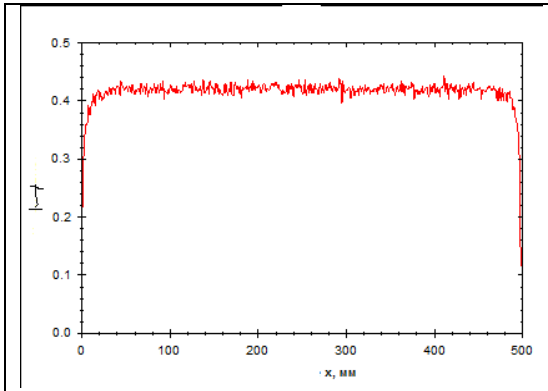

(I)

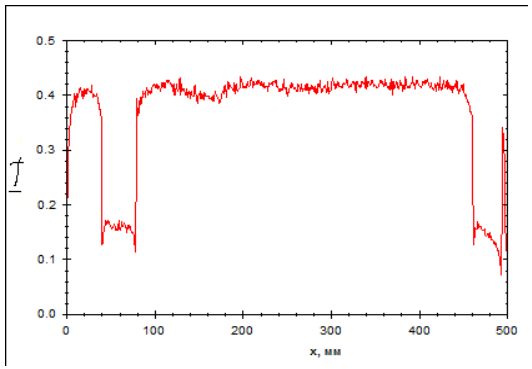

(II)

(a)Fiber glass of dimension (497mm by 18mm) at 3.00E+00 energy level

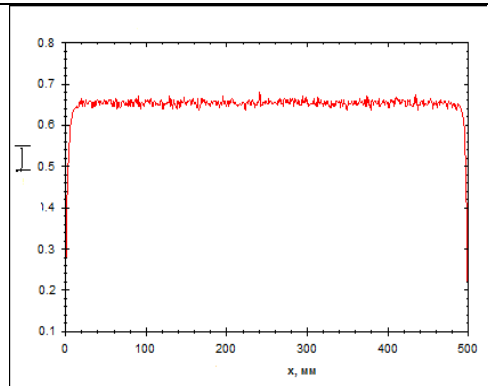

(I)

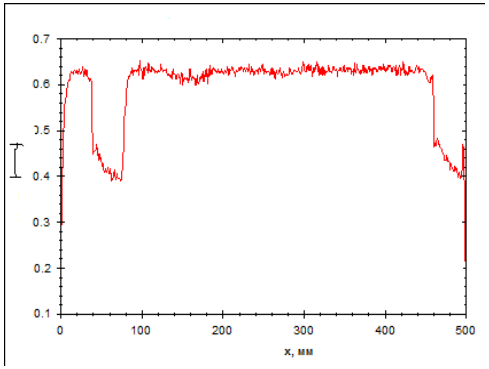

(II)

(b) Fiber glass of dimension (497mm by 98mm) at 3.00E+00 energy level

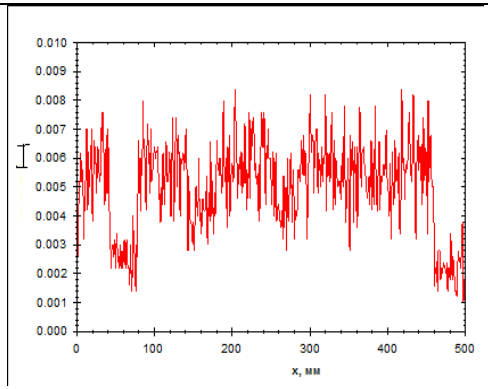

(I)

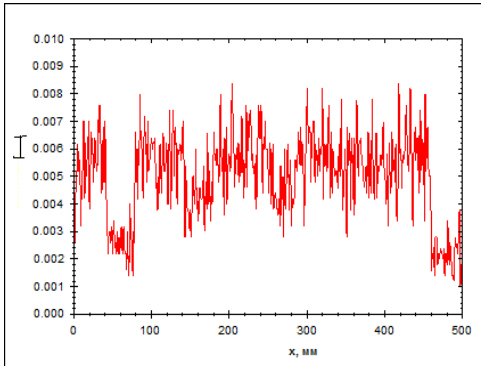

(II)

(c) Fiber glass of dimension (497mm by 98mm) at increased energy level(3.00E+03)

Fig. 8 Density variation in Fiber glass insulating material

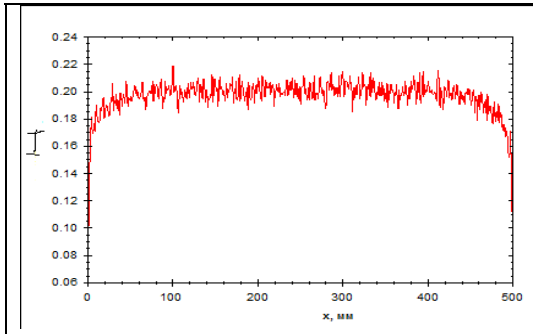

(I) without defects

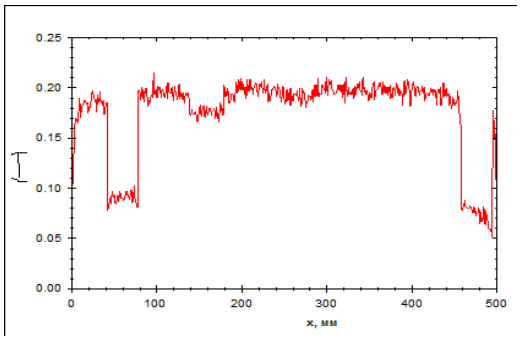

(II) with defects

(a) Epoxy material of dimension (497mm by 18mm) at 3.00E+00 energy level

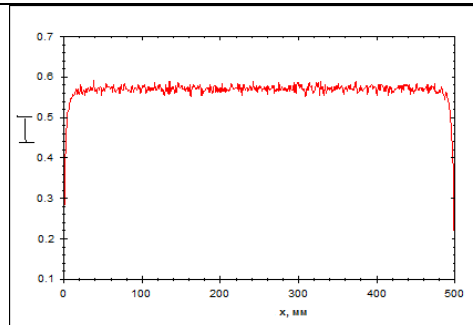

(I) without defects

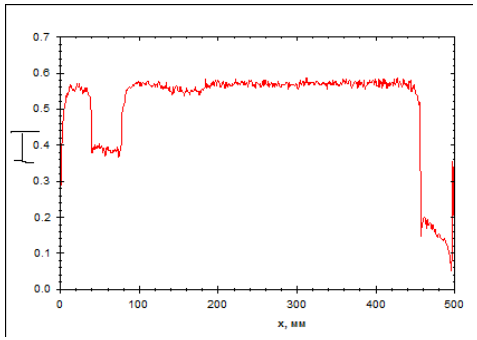

(II) with defects

(b) Epoxy material of dimension (497mm by 98mm) at 3.00E+00 energy level

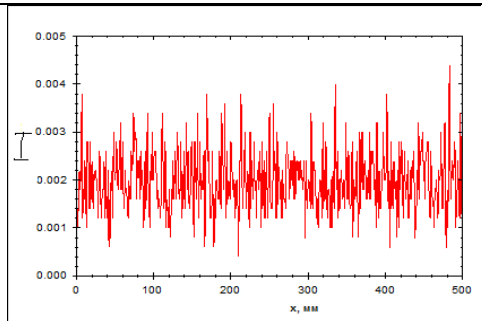

(I) without defects

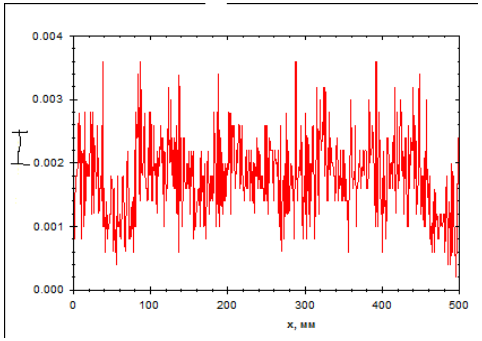

(II) with defects

(c) Epoxy material of dimension (497mm by 98mm) at increased energy level(3.00E+03)

Fig. 9 Density variation in Epoxy insulating material

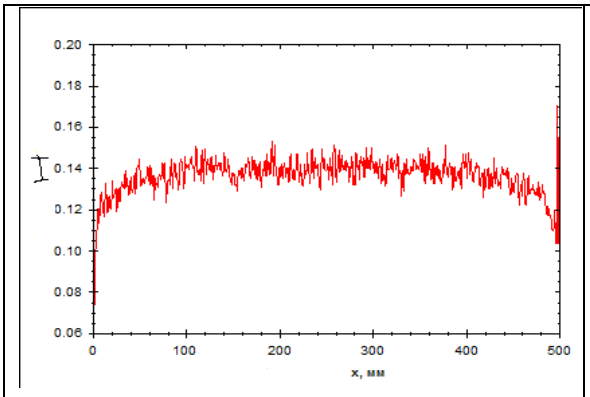

(I) without defects

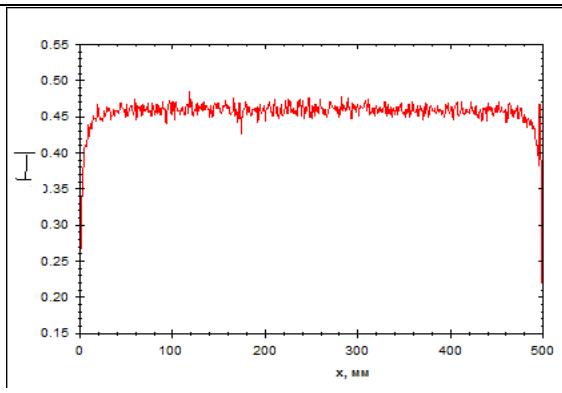

(I) without defects

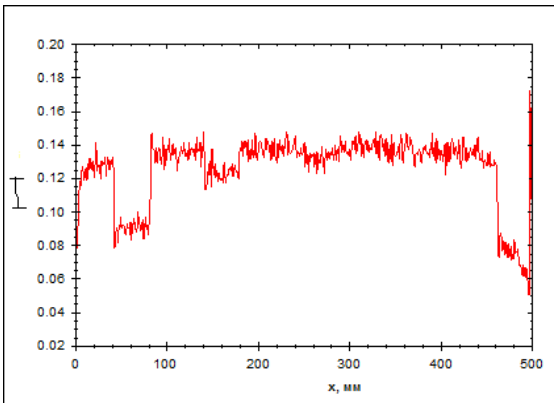

(II) with defects

(a) polyuthane foam material of dimension (497mm by 18mm) at 3.00E+00 energy level

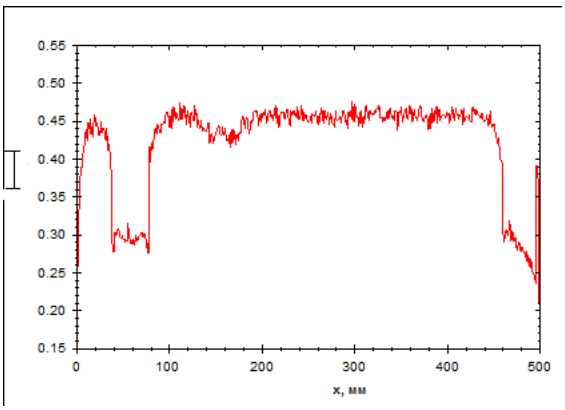

(II) with defects

(b) polyuthane foam of dimension (497mm by 98mm) at 3.00E+00 energy level

Fig. 10 Density variation in polyuthane foam

7. Conclusions

X-ray high level model which successfully demonstrates the behavior of x-ray backscattering analysis of thermal flaws in rocket combustion chamber has been developed. The model has proven to be reliable, precise and accurate in the analysis of thermal flaws in rocket combustion chamber wall.

References

1. Benjamin, T. A. Characterization and Optimization of Radiography by Selective Detection Backscatter X-Ray Imaging Modality. A Thesis Presented to the Graduate School of the University of Florida in Partial Fulfillment of the Requirements for the Degree of Master of Engineering University Of Florida, 2006.

2. Daniel, S., Edward, T. D., Alan, M. J. and Laurent, H. Preliminary Measurements Supporting Reactor Vesseland Large Component Inspection Using X-Ray Backscatter Radiography by Selective Detection, University of Florida, 202 NSC, Gainesville FL, 32611, Tel: 352-392-1401, Fax: 352-392-3380, 2004.

3. Dugan, E., Jacobs, A., Houssay, L. and Ekdahl, D. Detection of Flaws and Defects Using Lateral Migration X-ray Radiography. *Proceedings of SPIE 48th Annual Meeting, Symposium on Optical Science and Technology, Penetrating Radiation Systems and Applications,* Vol. 5199, pp. 47-61, San Diego, 2003.

4. Dugan, E., Jacobs, A., Su, Z., Houssay, L., Ekdahl D. and Brygoo, S. Development and Field Testing of a Mobile Backscatter X-ray Lateral Migration Radiography Land Mine Detection System. *SPIE Proceedings on Detection and Remediation Technologies for Mines and Mine like Targets VII*, Vol. 4742, pp. 120-131, Orlando, 2002.

5. Dugan, E., Jacobs, A., Shedlock, D. and Dan Ekdahl. Detection of Defects in Foam Thermal Insulation Using Lateral Migration Backscatter X-ray Radiography. *Proceedings of SPIE 49th Annual Meeting, Symposium on Optical Science and Technology, Penetrating Radiation Systems and Applications VI*, Vol. 5541, Denver, August, 2004.

6. Gouskov, O.V. and Kopchenov, V.I. Numerical investigation of gas-dynamic structure in the duct at supersonic conditions at the entrance. *Aeromechanika i Gasovaya Dinamika,* No.1, pp. 28-39, 2001.

7. Kolesnikov, A.I. and Leontiev, M. Machinery Encyclopedia. Theoretical Mechanics, Thermodynamics, Heat Transfer. *Machinery*, Vol.40, pp.600, Russian, 1999.

8. Maria L.S., Cristiano, V.D., Arthur B.B. and José W.M. CFD Analysis of the Combustion, Gas Flow, and Heat Exchange Processes in a boiler of a Thermal Power Plant. *Research Group of Energy Production Systems*, Catholic University of Rio Grande do Sul Av. Ipiranga, 6681, 90619-900, Porto Alegre–RS–Brasil, 2007.

9. Mikhatuli, D.S., Polezhaev, Y.V. and Reviznikov, D.L. Thermo-Erosion Destruction of Materials in Supersonic Heterogenous Flows. *European Conference for Aerospace Science (EUCASS)*, Section 4.4, pp.1-9, Moscow, 2005.

10. NIST Data website-http://physics.nist.gov/PhysRefData/Xcom/html/xcom1.html.

11. Olayiwola, R.O. A Numerical Simulation Model for in situ Combustion Process with Heat Source/Sink and Variable Permeability. *Journal of Modern Mathematics and Statistics,* 2(1),pp. 30-35, 2008.
12. Shivalinge, G., Krishnaveni, S., Yashoda, T., Umesh, T.K and Ramakrishna, G. Photon Mass Attenuation Coefficients, Effective Atomic Numbers and Electron Densities of Some Thermoluminescent Dosimetric Compounds, June, 2004.
13. Su Z., Jacobs, A., Dugan, E. and Ekdahl, D. X-Ray Lateral Migration Radiography System for the Application of Landmine Detection. *Proceedings of SPIE 45th Annual Meeting International Symposium on Optical Science and Technology*, Vol. 4142, pp. 150-160, San Diego, July, 2000.
14. White, G., Mathews, C., and King, L. Summary of USPWR Reactor Vessel Head Nozzle Inspection Results. Conference on Vessel Penetration Inspection, Crack Growth and Repair, 2003.
15. Hubbell, J. H., Veigele, W. J. Briggs, E. A. Brown, R. T. Cromer, D. T. and Howerton, R. J.Atomic Form Factors, Incoherent Scattering Functions, and Photon Scattering Cross Sections. *Jounal of. Physis and Chemistry.* Vol 4, p. 471, 1975.
16. Evans, R. D., *The Atomic Nucleus* (Kreiger, Malabar, FL, 1982);
17. Evans, R. D., "The Compton Effect," in S. Flugge, Ed., *Handbuch der Physik*, vol. 34 (Springer-Verlag, Berlin, 1958), p. 218;
18. Veigele ,W. J., Tracy , P. T., and Henry, E. M., "Compton Effect and Electron Binding," *Am. J. Phys.* **34**, 1116 , 1966.
19. Hubbell, J. H., Gimm, H. A., I., "Pair, Triplet, and Total Atomic Cross Sections (and Mass Attenuation Coefficients) for 1 MeV–100 GeV Photons in Elements Z = 1 to 100," *J. Phys. Chem. Ref. Data*, 9, 1023 , 1980.